THE JOURNAL OF PHYSICAL CHEMISTRY B

Article

pubs.acs.org/JPCB

Structural, Dynamical, and Thermodynamical Properties of Carbon Nanotube Polycarbonate Composites: A Molecular Dynamics Study

Souvik Chakraborty and Sudip Roy*

Physical Chemistry Division, National Chemical Laboratory, Pune 411008, India

Supporting Information

ABSTRACT: All-atom molecular dynamics simulations are performed on pure monomer and trimer of polycarbonate and their mixtures with different molecular weight percentages of embedded single walled carbon nanotubes at different temperatures to study the structural and dynamical properties of the composite system. The diffusion behaviors of monomer, trimer of polycarbonate and carbon nanotubes in composite matrices are investigated and compared with pure matrices in details. Both structural and dynamical properties indicate the weak interaction between the nanotubes and matrix molecules. The high tendency of nanotubes to form bundles is observed during simulation. The bundle formation free energy has been calculated from the potential of mean force calculations. The mechanism and energetics of bundle formation is explored in the atomistic scale. The formation of the carbon nanotube bundle is a favorable process in the oligomeric polycarbonate matrix.

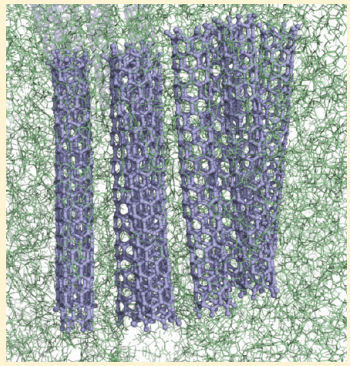

INTRODUCTION

For the past few years, carbon nanotube (CNT)−polymer composites have become an important field of study due to the improved structural and mechanical properties and the wide scope of applications in material sciences. A great deal of study, experimental as well as theoretical, has been performed and is going on this field to explore and analyze the structure and dynamics of nanocomposites. Polycarbonates are widely used as plastic material and have become very important industrially due to their good thermal and electrical resistivity and transparency. It has been observed that incorporation of CNTs in the polymer matrix can significantly enhance mechanical (strength and stiffness), thermal, and electrical properties of the polymer, and thus, CNTs can be used as a potential reinforcing agent.[1−8] CNTs in polymer matrix provide large interfacial area, and the nature of interactions in this interface region plays a crucial role in determining the improvements in the mechanical and dynamical properties of nanocomposites.

Polycarbonate nanocomposites were first synthesized by Zhao et al.[9] by solution mixing and were characterized by Raman spectroscopy. Potschke et al.[10] investigated distribution and alignment of CNTs in polycarbonate composites by statistical analysis of transmission electron microscopy (TEM). The correlation function was used to measure CNT clustering quantitatively and to derive local orientation factors. The study revealed that electrical conductivity can be enhanced by CNT clustering and reduced by alignment of tubes. Starr et al.[2] have investigated the influence of shape of nanoparticles on the viscosity of polymer−nanoparticle melt mixtures at high temperature and tensile strength in the ideal glass state by coarse-grain MD. Ruoff et al.[11] studied the sheathing of polymer in MWCNT−polycarbonate composites by scanning electron microscopy (SEM). They have found substantial evidence that suggests multiple polymer layers sheath nanotubes giving direct evidence for tube−polymer interaction. Argon et al.[12] performed quasi-static simulation on glassy bisphenol A polycarbonate with a static atomistic model to investigate the phenylene ring flip, conformational changes associated with the carbonate group, and the influence of the cooperative effect on main-chain dynamics. Fan et al.[13] used a modified version of Dreiding force field. The validity of this modified force field obtained by optimization of a few parameters by ab initio calculations was tested on a model polycarbonate compound and matched with crystallographic data. To propose a mechanism for the infrequent phenyl ring π-flips in polycarbonate was a challenging job. For this, instead of Newton's equation, Whitney and Yaris[14] have used the Langevin equation as the equation of motion to simulate phenyl ring flips in glassy polycarbonate. Eilhard, Zirkel, and co-workers[15] combined neutron scattering and computer simulations to gain deeper insight into the structure of polycarbonate melt. For simulation, they have introduced coarse graining to get a mesoscopic model from an atomistic model. Meyer et al.[16] developed two all-atom force fields for diphenyl carbonate (DPC), which is the main building block of the polycarbonate. One was derived from Hartree−Fock calculations and the other was from DFT calculations. Then, they have performed a simulation using these force fields separately to evaluate the structure and dynamics of liquid DPC over a wide temperature range and compared the data obtained by these two force fields. Müller-Plathe et al.[17] proposed a new

Received: December 19, 2011
Revised: February 14, 2012
Published: February 16, 2012

mechanism for diffusion of phenol molecules in bisphenol A–polycarbonate melt using MD simulation. This mechanism is different from that of smaller gaseous molecules that are known to penetrate the polymer matrix by hopping between pre-existing voids. The analysis revealed a transition from hopping diffusion toward more continuous diffusion at higher temperatures than 500 K. Kremer et al.[18] used coarse-grained MD simulations of polycarbonate to investigate chain dynamics, intramolecular structure, determination of entanglement molecular weight, and so forth.

Polymer nanocomposites are the new materials and getting lot of attention due to their tunable properties by changing the mixing ratios and mixing procedure of nanoparticles in the polymer matrix. Study of structural and dynamical properties of CNT–polycarbonate composite was not done before theoretically. In this paper, we have studied the structure and dynamics of nanocomposites by simulating single wall carbon nanotube (SWCNT)-dispersed monomers and trimers of polycarbonate by fully atomistic molecular dynamics (MD) simulation. In experiments,[19−25] it is a quite common feature of CNTs to agglomerate due to a strong cohesive force between CNTs. No studies on the mechanism and energetics of bundle formation of SWCNTs in the monomeric and oligomeric polycarbonate matrix have been done until now. We have explored the mechanism and energetics of bundling of CNTs in the matrix for the first time to the best of our knowledge.

COMPUTATIONAL DETAILS

Molecular Dynamics (MD) simulations of pure monomer and trimer of amorphous polycarbonate and systems mixed with different molecular weight percentages of SWCNTs have been studied with an all-atom force field using MD code GROMACS 4.0.7.[26,27] The total potential energy we have used is the sum of harmonic bond angle potential, proper dihedral potential with both periodic and Ryckaert–Bellemans[28,29] forms, improper dihedral potential, nonbonded interactions consisting of Lennard–Jones potential, and point-charge electrostatics.

As discussed above, Meyer et al.[16] and Müller-Plathe et al.[17] studied the properties of diphenyl carbonate (DPC) and bisphenol-A (BPA), respectively. Most of the bonded and nonbonded parameters are taken from these two papers. Meyer et al.[16] developed two sets of partial charges and proper dihedral parameters for DPC and studied physical properties using two sets of parameters. We have adopted the second set of the force field parameters (which they have recommended) for that part of our monomer structure (Figure 1), which is similar to the diphenyl carbonate. For the isopropyl part of the monomer (Figure 1), we have taken parameters (except partial charges) from Müller-Plathe et al.[17] For the determination of partial charges for the isopropyl group, we have calculated electrostatic potential (ESP) with B3LYP and 6-311G** basis set (same as Meyer et al. has done for DPC) using GAUSSIAN 09.[30] We have adopted partial charges for the atoms of the isopropyl group and for C_3, C_4, C_5, H_3, and H_5 from this calculation. For the rest of the atoms, we have kept the partial charges intact as reported by Meyer et al.[16] for DPC. Some partial charges are adjusted carefully to maintain overall charge neutrality for monomer and trimer units.

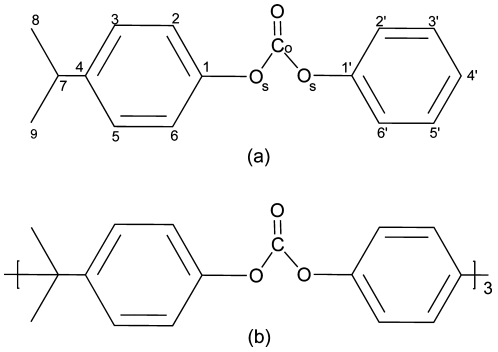

Figure 1. (a) Structure of monomer unit with atom numbering as used in the text. Hydrogen atoms carry the label number of carbon atoms to which they are attached. (b) Structure of trimer unit.

All the force field parameters used for monomer and trimer are given in Tables 1–5 in the Supporting Information. The bond angle and angle constants of C_4–C_7–H_7 and $C_{8,9}$–C_7–H_7, and the proper dihedral (Ryckaert–Bellemans) parameters are taken from OPLS[31,32] force field. We have excluded all 1–4 nonbonded interactions and kept bond lengths constant in accordance with Meyer et al.[16] For the CNT, we have used OPLS[31,32] force field parameters. Charges on the atoms of the nanotube are taken as zero.

We have prepared a system of pure monomers at 500 K and gradually cooled down by 20 K to 380 K. Simulated annealing is performed by raising the temperature from 500 to 1000 K and cooling down to 500 K with steps of 25 K and an annealing time of 25 ps. Approximately 2%, 5%, and 10% by molecular weight of SWCNT–monomer mixtures are prepared at temperatures of 500, 480, and 460 K. 2%, 5%, and 10% mixtures contain 5, 10, and 15 SWCNTs, respectively. We have taken a zigzag single walled CNT of diameter 4.69 Å and length 40.7 Å consisting of 240 atoms. We have used Berendsen[33] thermostat with a coupling time of 0.2 ps and Berendsen barostat with pressure of 1 bar. Isotropic pressure coupling is used with coupling times of 1.5 ps. Periodic boundary conditions are applied in all three directions for all the systems. Bond lengths are kept constant using LINCS algorithm.[34] Reaction field electrostatics is used with a cutoff length of 1.2 nm and dielectric constant, $\varepsilon_{RF} = 3.5$. The integration time step is 2 fs. The monomeric systems are pre-equilibrated for 1 ns, equilibrated for 10 ns, and the final production run is performed for another 10 ns at three different temperatures.

For trimer, we have prepared the pure trimer system at 520, 500, 490, 480, 460, and 440 K. Simulated annealing is performed to sample the phase space properly because of long chains of the oligomers. In simulated annealing, the temperature is raised from 500 to 900 K and cooled down to 500 K with a step of 40 K. The annealing time for each step is 400 ps. Systems are equilibrated for 40 ns, and production runs are performed for an additional 50 ns. 2%, 5%, and 10% of SWCNT–trimer mixtures are also prepared at 500, 480, and 460 K in a similar way. The number of CNTs in three different mixtures are the same as in the case of CNT–monomer mixtures. These mixed systems are subjected to an equilibration run for 30 ns and a production run for additional 20 ns. Temperature coupling is used with coupling times of 0.1 ps. All other control parameters for MD are the same as in the case of the monomer systems.

To validate the force fields, we focused on two properties to examine, density and glass transition temperature. We have calculated the densities at different temperatures and plotted as a function of temperature for both pure monomer (Figure 2a) and trimer (Figure 2b) and compared the densities with the densities (both experimental and theoretical) of DPC as

dx.doi.org/10.1021/jp212220m | J. Phys. Chem. B 2012, 116, 3083–3091

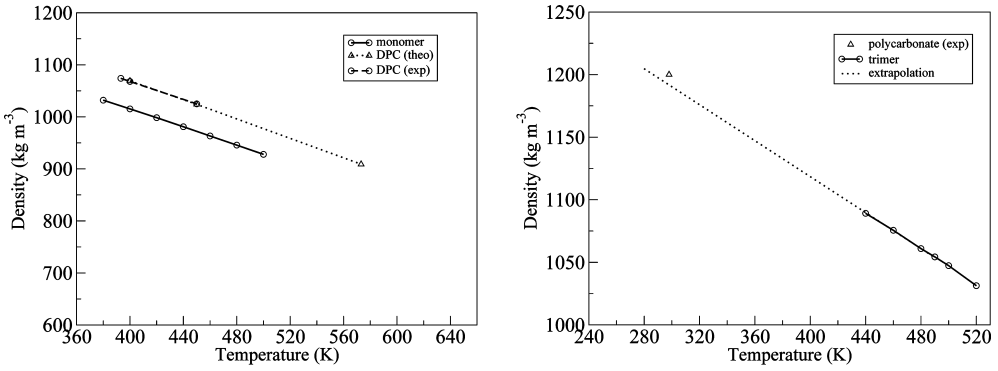

Figure 2. (a) Density of pure monomer as a function of temperature along with the theoretical and experimental densities of DPC. (b) Density of pure trimer as a function of temperature with experimental value of density of polycarbonate.

reported by Meyer et al.[16] From Figure 2a, we can see that DPC has higher densities (both experimental and theoretical) than the densities of pure monomer we have calculated theoretically. But in the case of the pure trimer system, when we have done linear fitting of the density as a function of temperature plot between 490 and 440 K and extrapolated it (Figure 2b), the extrapolated straight line passed very close to the experimental density of polycarbonate[35] at room temperature. To find the glass transition temperature and compare with the experimental value, we have calculated diffusion coefficients at different temperatures for the pure trimer system. The experimental glass transition temperature for polycarbonate is 418−432 K.[36−38] To find the diffusion coefficient of the trimer at each temperature, mean square displacement (MSD) is plotted for every 10 ns of trajectory starting from 40 to 90 ns and then averaged over to get an average MSD reported in the Supporting Information (SI Figure 1). Natural logarithm of diffusion coefficients as a function of inverse of temperature has been shown in Figure 3 and linear fitting has been done between 520 and 490 K and another between 490 and 440 K. In Figure 3, it is observed that a steep decrease in diffusion coefficient starts near 490 K, which indicates that the glass transition temperature is near to 490 K. In comparison to the experimental glass transition temperature for polycarbonate, the deviation is less than 15%. As we are simulating oligomeric polycarbonate, the 15% deviation in glass temperature is acceptable.

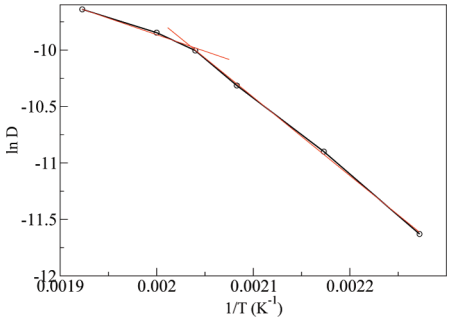

Figure 3. Natural logarithm of diffusion coefficients as a function of inverse of temperature for pure trimer.

RESULTS AND DISCUSSION

Structural Properties. To investigate the structural environment around the CNT in monomer and trimer mixtures, the radial distribution function (RDF) is calculated between CNT's carbons and four types of atoms of monomer and trimer: carbonyl oxygen, carbonyl carbon, bridge oxygen, and aromatic carbon at 500 K for three different mixtures (2%, 5%, 10%) depicted in Figures 4 and 5. For 2% mixtures of both

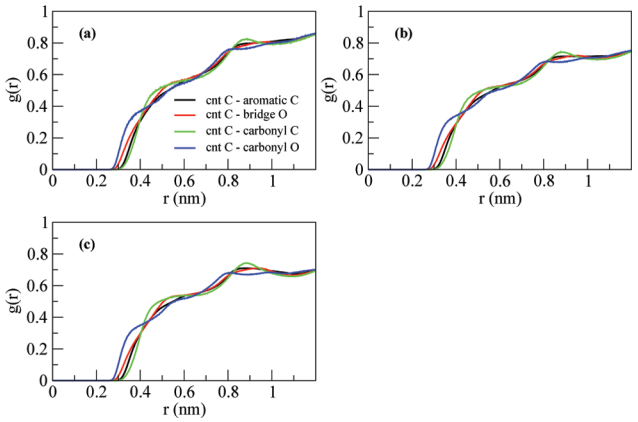

Figure 4. RDFs between the carbonyl oxygen of the monomer and CNT carbons, the bridge oxygens of the monomer and CNT carbons, the carbonyl carbons of the monomer and CNT carbons, the aromatic carbons of the monomer and CNT carbons. (a) 2% mixture, (b) 5% mixture, and (c) 10% mixture.

monomer and trimer, we see that minima of first peaks for carbonyl oxygen, bridge oxygen, carbonyl carbon, and aromatic carbon are approximately at 0.45, 0.65, 0.70, and 0.70 nm, respectively. For the carbonyl oxygen, the second minimum is at ∼0.66 nm. For the carbonyl carbon, the second minimum is observed at ∼1.05 nm. For 5% and 10% mixtures, these distances are also almost the same. The structural environment around CNTs is not changing with CNT content, and it remains the same if we go from monomer to trimer matrix. The absence of any sharp peak in RDF plots indicates that the interaction between CNT carbons and these four types of atoms of the matrix molecules is less attractive in nature. There is almost no wetting of molecules, and therefore, CNTs have high tendency to self-assemble, which leads to the formation of bundles.

dx.doi.org/10.1021/jp212220m | J. Phys. Chem. B 2012, 116, 3083−3091

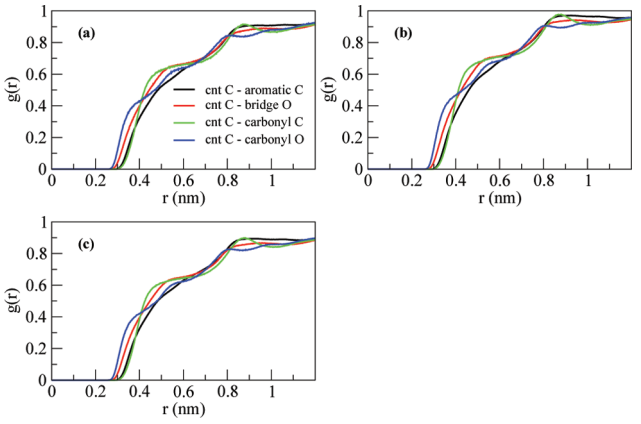

Figure 5. RDFs are the same as in Figure 4 but for CNT−trimer composite system. (a) 2% mixture, (b) 5% mixture, and (c) 10% mixture.

Mean Square Displacement. The dynamical as well as rheological properties of polymers incorporated with nanomaterials have been studied previously experimentally and theoretically.[1−3,39] Wei et al.[39] studied the diffusion behaviors of pure polyethylene (PE) and CNT−polyethylene composite by molecular dynamics (MD) using united atom force field and found that the diffusion coefficient of polyethylene has increased from the pure polymer to the CNT−polymer composite at a fixed temperature. They have explained it on the basis of thermal expansion coefficient. Increased thermal expansion of the composite enhanced the diffusivity of the polymer above the glass transition temperature. Their study also showed that, with increase in temperature, the diffusion coefficient of the polymer increases for both pure and mixed systems.

Figure 6a,b shows the mean square displacement (MSD) of the center of mass of the monomer and the trimer, respectively, in different mixtures at three different temperatures. The slope of the graph is decreasing with a decrease in temperature for a fixed percentage mixture. Due to the decrease in kinetic energy of the molecules with the decrease of temperature, diffusivity of the molecule gets lowered. The slope of the MSD graphs (Figure 6a,b) also decreases with the increase in CNT content in the matrix. Interestingly, pure monomer and trimer systems have lower slopes for MSD than 2% CNT−monomer/trimer composites. To compare the self-diffusion behavior of the centers of masses of the monomer and the trimer in pure system and three different mixtures of CNT−monomer and CNT−trimer at three different temperatures, we have calculated diffusion coefficients from the average MSD (Figure 6a,b) calculated from 5 sets of 2 ns trajectories of production run . When we compared the diffusion coefficients of pure monomer and 2% mixture at different temperatures, we have observed the increase in the diffusion constant, as reported in Table 1. In the case of trimer systems (Table 2), increase in diffusion coefficients is also observed when we have compared between the pure and the 2% mixture system. However, with the increase in CNT content, that is, in 5% and 10% systems, the diffusion constant for monomer and trimer decreases. For 5% and 10% mixed systems, the glass transition temperature may have increased (the glass transition temperature of pure trimer is 490 K), and this may be a reason for the decrease of diffusion coefficient. As it is computationally costly to simulate different mixed systems for wide range of temperatures, the investigation of glass transition temperature for mixed systems has not been performed presently. In experiments, viscosities of different polymers embedded with nanoparticles or CNTs or nanofibres have been studied.[1,3] As it is difficult to measure viscosity with accuracy by fully atomistic molecular dynamics, we have not investigated viscous properties here.

To get better statistics of diffusivity of CNTs (as the number of CNT is less), we have plotted MSDs of CNTs at 2 ns intervals for 10 ns of production run and averaged over both in the case of monomer (Figure 7a) and trimer (Figure 7b) matrices. In the case of monomer matrices (Figure 7a), MSD plots are showing that diffusivity of the CNT decreases with increasing CNT percentage at a particular temperature. For 10% mixtures, diffusivity is quite low, and this fact can be attributed to the high tendency of bundle formation by the CNTs. In case of trimer matrices (Figure 7b), the diffusivity of the CNT is lower than that in the monomer. For initial 100−120 ps, the MSD plots are showing parabolic nature. This may be due to the fact that the trimer matrices have acquired some glassy behavior at these three temperatures and due to repulsive interaction between the CNT and the polymer, within this very short time period CNTs follow the path like straight line with constant velocity before facing collision with other CNTs. CNTs are also confined in the molecular matrix. The monomer matrix is much liquidlike, but the trimer matrix can create lot of confinement due to its long chains. Therefore MSD of only one of the CNTs over 10 ns production runs for each mixture at three different temperatures have been shown in Figure 7c,d for both the monomer and the trimer systems, respectively. The

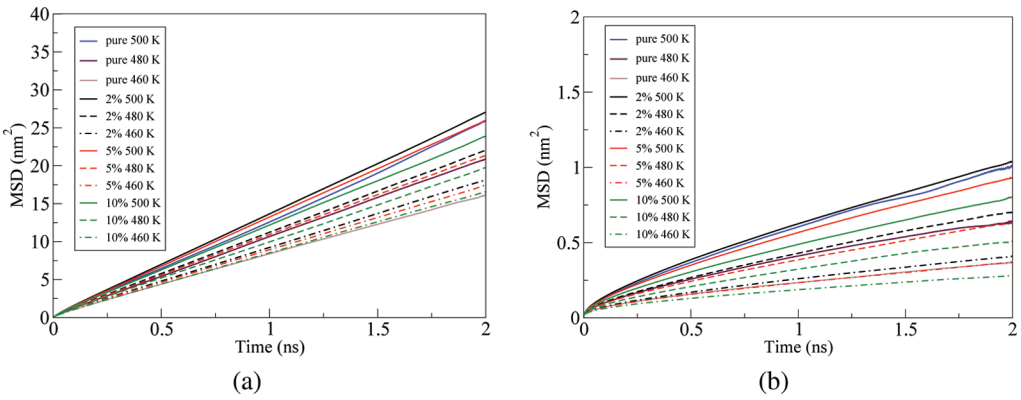

Figure 6. MSD plots for pure, 2%, 5%, and 10% mixtures for (a) monomer and (b) trimer at 500, 480, and 460 K.

dx.doi.org/10.1021/jp212220m | J. Phys. Chem. B 2012, 116, 3083−3091

Table 1. Diffusion Coefficients of Monomer (10^{-5} cm^2/s)

temp (K)	neat monomer	2%	5%	10%
500	2.0914 ± 0.0479	2.2124 ± 0.0545	2.1407 ± 0.0285	1.9543 ± 0.0922
480	1.7273 ± 0.0985	1.8090 ± 0.0646	1.7569 ± 0.0551	1.6047 ± 0.0372
460	1.3153 ± 0.1020	1.4869 ± 0.0299	1.4198 ± 0.0325	1.3647 ± 0.0657

Table 2. Diffusion Coefficients of Trimer (10^{-5} cm^2/s)

temp (K)	neat trimer	2%	5%	10%
500	0.0737 ± 0.0053	0.0757 ± 0.0030	0.0683 ± 0.0013	0.0581 ± 0.0031
480	0.0473 ± 0.0073	0.0518 ± 0.0015	0.0455 ± 0.0023	0.0368 ± 0.0024
460	0.0247 ± 0.0020	0.0282 ± 0.0011	0.0247 ± 0.0017	0.0182 ± 0.0011

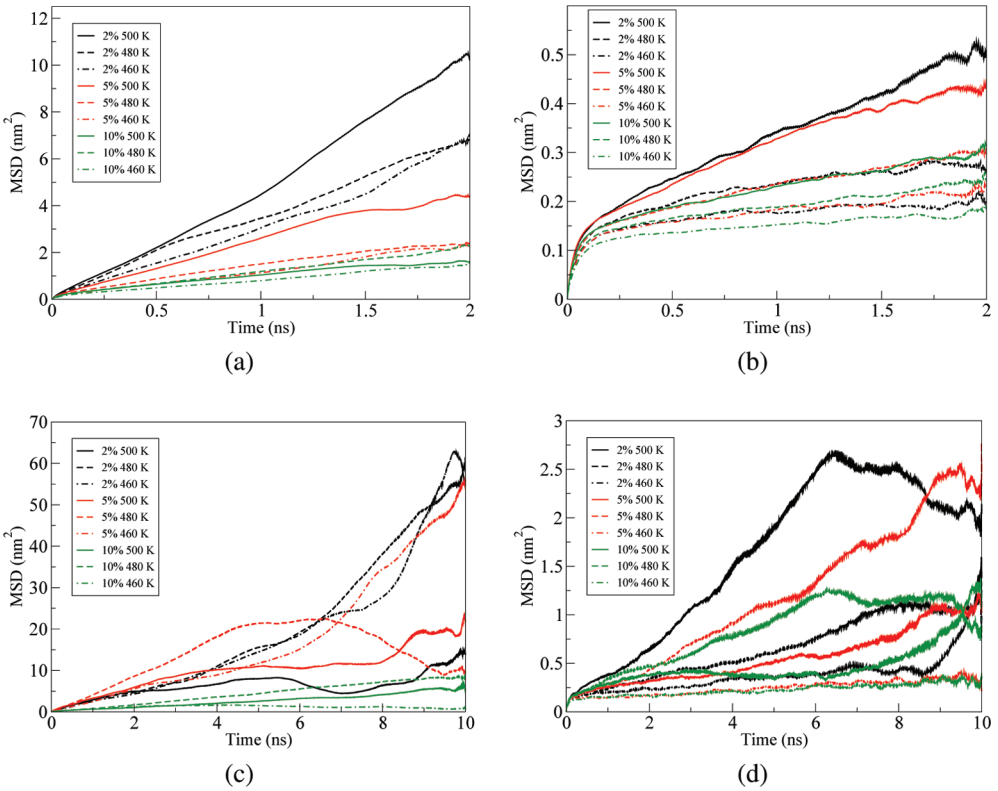

Figure 7. MSDs at 500, 480, and 460 K for 2%, 5%, and 10% mixtures for (a) all the CNTs in 2 ns intervals averaging over 10 ns in monomer matrix, (b) all the CNTs in 2 ns intervals averaging over 10 ns in trimer matrix, (c) only one of the CNTs in monomer matrix for 10 ns of production run, and (d) only one of the CNTs in trimer matrix for 10 ns of production run.

graphs are quite nonlinear in pattern, and some of them intercross each other. This behavior of diffusion of CNTs indicates the confined motion of CNTs in the matrices.

Like in monomer matrices, diffusivity of CNTs is decreasing with higher CNT content. The probability of bundle formation increases with a higher number of CNTs, and therefore, the diffusivity of CNTs gets decreased. While investigating the dynamics of CNTs in the matrix for monomer systems, we have found that CNTs are aligned in parallel fashion and agglomerating with each other. In a 10% mixture of monomer, we have clearly observed the formation of bundles and alignment of CNTs in parallel fashion. The agglomeration of CNTs in the polymer composite is reported experimentally.[19−25] Due to high cohesive energy, CNTs tend to agglomerate in polymer melt. This bundle formation phenomena propelled us to investigate the mechanism associated with and the energetics that can explain the alignment and agglomeration of CNTs in composite.

Bundle Formation: Mechanism. To represent the mechanism of bundle formation and the structural changes in the CNT−monomer interface regions while bundle formation is going on (when equilibrating the system), we have examined the structural changes surrounding CNTs. For this, we have chosen 1−21 ns trajectory of a 10% mixture of monomer−CNT at 500 K as this system consists of a maximum number of CNTs. To examine the probability that the center of masses of CNTs are coming closer with time, the cutoff distance between the center of masses of CNTs is taken as 2 nm, which is a reasonable approximation to explore bundling formation phenomena. At each frame, the distances between all the CNTs have been calculated, and the number of distances whose value falls below 2 nm were calculated and divided by the total number of probable distances. Figure 8 represents how the probability that the center of masses of CNTs coming closer is changing with time. We can see that the probability is increasing with time, which indicates that the CNTs are

dx.doi.org/10.1021/jp212220m | J. Phys. Chem. B 2012, 116, 3083−3091

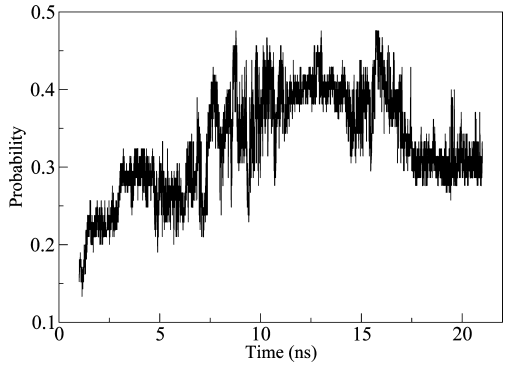

Figure 8. Probability of CNT center of masses coming within the distance of 2 nm as a function of time.

coming close to each other with time leading to the bundle formation. Figure 9 shows the change of average angle between

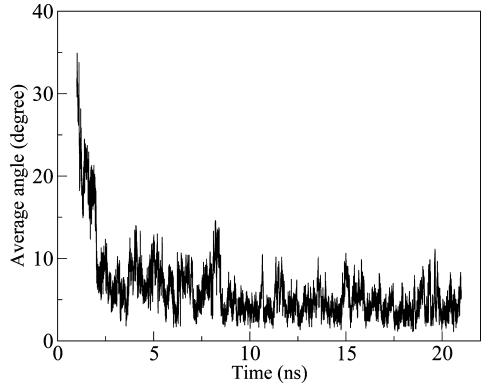

Figure 9. Change of average angle between the CNTs with time.

the CNTs with time. For this, each CNT is represented by a vector, and angles between the vectors were calculated at each frame only if the center of mass distance between the corresponding CNTs comes within cutoff distance of 2 nm. It shows that the average angle is rapidly decreasing with time and comes close to zero degree after 3−4 ns. Thus, it is clear that CNTs are not only coming close to each other with time, also they are aligning in a definite pattern that is parallel arrangement. Figure 10 represents the distribution of angles between the CNTs over 10 ns of production run considering the same cutoff distance between the center of masses of

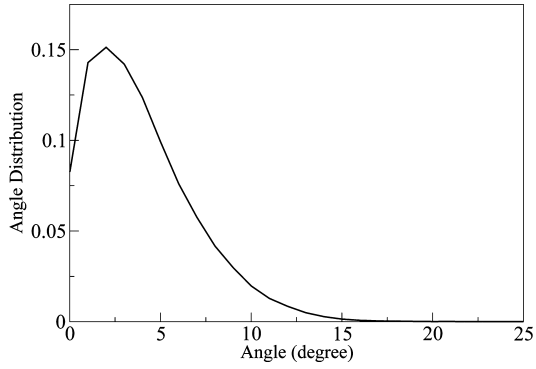

Figure 10. Distribution of angles between the CNTs for 10 ns production run of 10% at 500 K.

CNTs. A distinct peak appeared near 2° indicating clearly that the CNTs have high tendency to be aligned parallel while agglomerating. In Figure 11, a snapshot of equilibrated CNT−monomer system showing the bundle formation has been depicted.

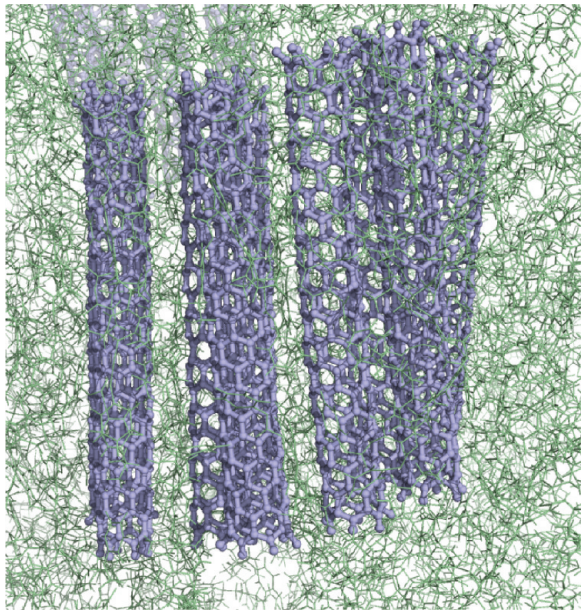

Figure 11. Snapshot of bundle of nanotubes in equilibrated 10% monomer matrix at 500 K.

The structural changes at the CNT−monomer interface during bundle formation has been investigated. We have selected four types of atoms of the monomer (carbonyl oxygen, bridge oxygen, carbonyl carbon, and aromatic carbon) to see how their spatial proximity with carbon atoms of the CNT changes with time. Each carbon atom of the CNT is considered as the center of a sphere with a definite radius within which the change of the average number of various atoms of monomer is determined. For the carbonyl oxygen, the bridge oxygen, the carbonyl carbon, and the aromatic carbon of monomer, graphs of radial distribution function with respect to the CNT carbon have been reported in Figures 4 and 5. For each type of atom, the distances at which the minima of first peaks (first solvation shell) have appeared in radial distribution plots are considered as the radius of the corresponding sphere. For a particular type of atom, the distances from each of the CNT carbons are calculated. Only those atoms are recognized whose distances from the CNT carbon fall within the defined radius at each time frame. Figure 12 shows the change of the average number of four types of atoms with time. All four plots are showing that average number is decreasing with time as CNTs are coming closer to each other to form bundles. In the case of the carbonyl oxygen (Figure 12a), we can see that the average number is quite less than the other three types of atoms at initial time and its decrease with time is small compared to the others. Due to less attractive interaction between the CNT carbons and the carbonyl oxygens, the number of carbonyl oxygens present in first solvation shell of the CNT carbons is very less, and hence, the decrease of the number of carbonyl oxygens during bundle formation is also insignificant. For the bridge oxygen (Figure 12b), the carbonyl carbon (Figure 12c), and the aromatic carbon (Figure 12d), the decrease in number with time is

dx.doi.org/10.1021/jp212220m | J. Phys. Chem. B 2012, 116, 3083−3091

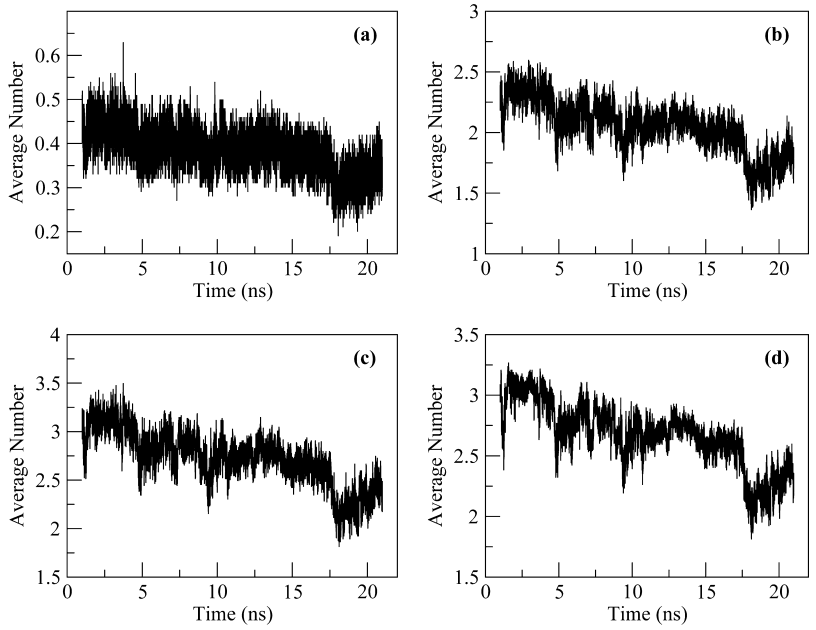

Figure 12. Change in average number of (a) the carbonyl oxygen, (b) the bridge oxygen, (c) the carbonyl carbon, (d) the aromatic carbon with time during bundle formation in a 10% CNT−monomer mixture at 500 K.

significant compared to the carbonyl oxygen. The number of bridge oxygen atoms shows higher decrease than the carbonyl oxygens. The carbonyl carbon and the aromatic carbon have almost a similar trend, and they have greater average value than both the bridge oxygen and the carbonyl oxygen. This comparison gives an idea how these four types of atoms participate in structural changes around the CNT carbons in the bundle formation process.

Bundle Formation Energetics: Umbrella Sampling. Umbrella sampling simulations are used to determine the free energy change (ΔG) associated with an event along a reaction coordinate, ξ.[40−42] This technique is useful in determining the binding energies and macromolecular interactions.[43−52] By umbrella sampling, a biasing potential is added to the Hamiltonian of the system to improve the sampling of the conformational space that are insufficiently sampled. A series of configurations is generated along a reaction coordinate, ξ, between two interacting species one of which is considered as a reference and the other one is subjected to a biasing potential. The species under biasing potential takes up different positions with increasing center of mass distance from the reference point. With the increasing center of mass distances, few configurations are extracted that are called "sampling windows". Then, for each window, independent simulation is performed to generate an ensemble of structures along the reaction coordinate. From each of these independent simulations, potential of mean force (PMF) is calculated and assembled over all the adjacent windows along the reaction coordinate by weighted histogram analysis method (WHAM) proposed by Kumar et al.[53] Gibb's free energy, ΔG, is calculated from the PMF curve.

To find the energetics of the bundle formation, we have performed umbrella sampling on the CNTs in both monomer and trimer matrices. It is also interesting to investigate how binding energy between CNTs changes if we go from monomer to trimer matrix. We have taken two types of arrangements of CNTs in the mixture and prepared two separate sets of rectangular boxes. In one of the boxes, two CNTs are placed parallel to each other, and in another one, they are placed in a perpendicular fashion. The center of mass distance is kept at approximately 0.8 nm. The aim of putting CNTs in two different conformations separately is to compare the corresponding free energy changes associated with two different types of approaches: parallel approach of one CNT to other one and the perpendicular approach of one to another in the composite. Each of the boxes is elongated along the z axis as one of the CNTs is pulled along the z axis. Initially, we have equilibrated the systems restraining two CNTs at their position for 10 ns for monomer matrix and 20 ns for trimer matrix at constant pressure (NPT) of 1 bar. The temperature is maintained at 500 K using a Berendsen thermostat. All other parameters used are the same as those used for CNT−monomer and CNT−trimer mixed systems described in the simulation details section. The structures generated at the end of the equilibration are used as the starting configurations for pulling simulations.

The pulling simulation for each of the mixed systems (one with two parallel CNTs and another with two perpendicular CNTs) has been performed. One CNT is position-restrained, and the other one is pulled along the z axis with restraints along the x and y axes. For monomer matrices, each of the pulling simulations is carried out with a pull force contant 700 kJ mol^{-1} nm^{-2} and pull rate of 0.01 nm ps^{-1}. For trimer matrices, the pull force constant is 600 kJ mol^{-1} nm^{-2}, and the pull rate is 0.01 nm ps^{-1}. The pull rates and pull force constants are optimized to get the best combination for the systems. For each system, one CNT is pulled away from a restraining one along the z axis over 0.5 ns. From these trajectories, 250 windows have been extracted. To choose the starting window, change in the center of mass distances between two tubes along the z axis are checked for each system. The starting window is selected from the region of coordinate where the center of mass distance between the two CNTs has started increasing significantly and if in the histogram of the configurations within the sampling windows there is sufficient overlap between the starting and the immediate adjacent window. The last window for sampling is

dx.doi.org/10.1021/jp212220m | J. Phys. Chem. B 2012, 116, 3083−3091

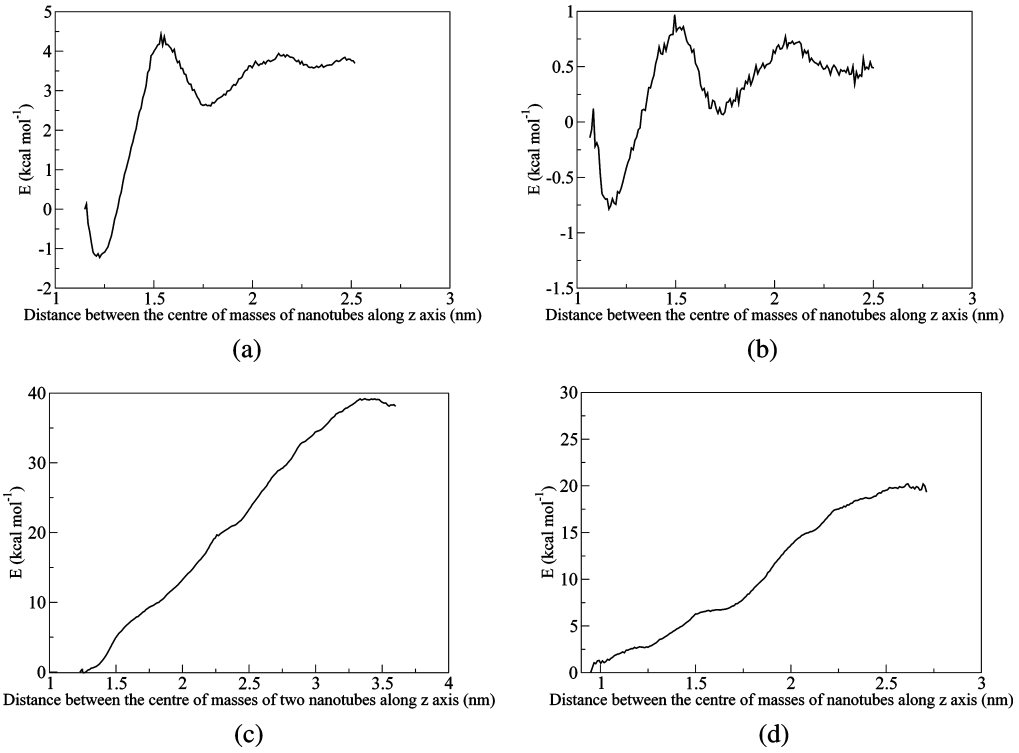

Figure 13. Potential of mean force (PMF) curves: (a) when pull is applied along the *z* axis on one of the parallel aligned CNTs in monomer matrix; (b) when pull is applied along the *z* axis on one of the perpendicularly aligned CNTs in monomer matrix; (c) when pull is applied along the *z* axis on one of the parallelly aligned CNTs in trimer matrix; and (d) when pull is applied along the *z* axis on one of the perpendicularly aligned CNTs in trimer matrix.

chosen until the plateau region in the potential of mean force (PMF) curve (Figure 13) has been achieved. For parallel tubes in monomer matrix, all the windows between 1.2 and 2.5 nm center of mass distance are chosen, and for perpendicular tubes, windows are chosen with a gap of approximately 0.1 nm center of mass distance between 1.2 and 2.5 nm. In the trimer system with parallel and perpendicular tubes, windows are selected between 1.3 and 3.4 nm and between 1.2 and 2.5 nm, respectively, keeping approximately a 0.1 nm gap. Each of the windows has been subjected to 5 ns of MD run. Finally weighted histogram method (WHAM)[53] is applied to get the binding energies.

The potential of mean force (PMF) curves (Figure 13) are obtained for each of the systems by applying the weighted histogram analysis method (WHAM)[53] on sampling windows for last 4.5 ns, and the free energy change (ΔG) for each system is calculated and summarized in Table 3. Histogram plots

Table 3. Binding Free Energies of CNTs from Umbrella Sampling (kcal mol^{-1})

system	parallel	perpendicular
monomer	−5.53	−1.72
trimer	−39.27	−20.10

(Supporting Information, Figure 2) show sufficient overlap between the adjacent windows. In monomer matrix, ΔG for parallel tubes (Figure 13a) is −5.53 kcal mol^{-1}, and for perpendicular tubes (Figure 13b), it is −1.72 kcal mol^{-1}. In the trimer system, binding energy has increased significantly. ΔG for parallel tubes (Figure 13c) is −39.27 kcal mol^{-1}, and for perpendicular tubes (Figure 13d), it is −20.10 kcal mol^{-1}.

From the umbrella sampling, we can interpret the energetics associated with the bundle formation mechanism for CNTs. Binding free energy is less for parallel alignment of nanotubes than perpendicular in both monomer and trimer matrices. Interestingly, binding free energy decreased significantly when the matrix is changed from monomer to trimer. Interaction between CNTs and the matrix plays quite a significant role in energetics of bundle formation. More polymeric solvent may enhance the binding energy, hence bundle formation.

CONCLUSIONS

Molecular dynamics simulation has been performed on pure and CNT mixed systems of monomer and trimer of polycarbonate at different temperatures. The structural environment remains intact for both monomer and trimer at three different mixtures of CNTs at three different temperatures (500, 480, 460 K). RDF plots indicate that less attractive interaction between the carbons of CNTs and atoms of matrix molecules predominates in the composite. Investigation of the diffusion behavior of solvent molecules in different mixtures reveals that, with increasing percentage of CNT at a fixed temperature, the diffusivity of solvent molecules decreases. MSD graphs of individual CNTs showed much nonlinearity due to their confined motion and bundle formation of CNTs has been observed in monomer matrices prominently in the case of a 10% mixture. Then, we have looked into the details of bundle formation mechanism analyzing a 10% mixed system at 500 K.

To explore the energetics of bundle formation, umbrella sampling technique has been used. Binding energy of CNT placed in parallel to each other is less than that of the perpendicular orientation. Binding energies have been

decreased from monomer to trimer mixture, which indicates that polymerization has a role to play in enhancement of binding energy. In the future, we can explore the binding energies for higher oligomeric units and also for different polymers for comparisons. The binding energies can be explored taking more number of CNTs and also for different aspect ratio and chirality. The tendency of CNTs to form bundles leads us to believe that there is a high probability of formation of percolation network between the bundles in the polymer matrix that can be explored with the help of multiscale modeling such as coarse-graining.

■ ASSOCIATED CONTENT

Supporting Information

Tables of force field parameters, average mean square displacement plot for pure trimer at different temperatures to find glass transition temperature, and histograms from umbrella sampling. This material is available free of charge via the Internet at http://pubs.acs.org.

■ AUTHOR INFORMATION

Corresponding Author

*E-mail: s.roy@ncl.res.in; Phone: +91 (020) 25902735; Fax: +91 (020) 25902636.

Notes

The authors declare no competing financial interest.

■ ACKNOWLEDGMENTS

We gratefully acknowledge DST (project code SR/FT/CS-021/2009) for financial support for the project. Author S.R. gratefully acknowledges center for excellence in scientific computing, NCL, for significant amount of computational time.

■ REFERENCES

(1) Potschke, P.; Fornes, T. D.; Paul, D. R. *Polymer* **2002**, *43*, 3247−3255.
(2) Starr, F. W.; Knauert, S. T.; Douglas, J. F. *J. Polym. Sci., Part B: Polym. Phys.* **2007**, *45*, 1882−1897.
(3) Lozano, K.; Bonilla-Rios, J.; Barrera, E. V. *J. Appl. Polym. Sci.* **2001**, *80*, 1162−1172.
(4) Lozano, K.; Barrera, E. V. *J. Appl. Polym. Sci.* **2001**, *79*, 125−133.
(5) Subramoney, S. *Adv. Mater.* **1998**, *10*, 1157−1171.
(6) Dickey, E. C.; Qian, D. *Appl. Phys. Lett.* **2000**, *76*, 2868−2870.
(7) Coleman, J. N.; Gun'ko, Y. K.; Khan, U. *Adv. Mater.* **2006**, *18*, 689−706.
(8) Coleman, J. N.; Cadek, M.; Blake, R.; Nicolosi, V.; Ryan, K. P.; Belton, C.; Fonseca, A.; Nagy, J. B.; Gun'ko, Y. K.; Blau, W. J. *Adv. Funct. Mater.* **2004**, *14*, 791−798.
(9) Zhao, Q.; Wood, J. R.; Wagner, H. D. *J. Polym. Sci., Part B: Polym. Phys.* **2001**, *39*, 1492−1495.
(10) Potschke, P.; Pegel, S.; Villmow, T.; Stoyan, D.; Heinrich, G. *Polymer* **2009**, *50*, 2123−2132.
(11) Ruoff, R. S.; Ding, W.; Eitan, A.; Fisher, F. T.; Chen, X.; Dikin, D. A.; Andrews, R.; Brinson, L. C.; Schadler, L. S. *Nano Lett.* **2003**, *3*, 1593−1597.
(12) Argon, A. S.; Hutnik, M.; Suter, U. W. *Macromolecules* **1991**, *24*, 5970−5979.
(13) Fan, C. F.; Cagin, T.; Chen, Z. M. *Macromolecules* **1994**, *27*, 2383−2391.
(14) Yaris, R.; Whitney, D. R. *Macromolecules* **1997**, *30*, 1741−1751.
(15) Eilhard, J.; Zirkel, A.; Tschop, W.; Hahn, O.; Kremer, K.; Scharpf, O.; Richter, D.; Buchenau, U. *J. Chem. Phys.* **1999**, *110*, 1819−1830.
(16) Meyer, H.; Hahn, O.; Muller-Plathe, F. *J. Phys. Chem. B* **1999**, *103*, 10591−10598.
(17) Müller-Plathe, F.; Hahn, O.; Mooney, D. A.; Kremer, K. *J. Chem. Phys.* **1999**, *111*, 6061.
(18) Kremer, K.; Delle Site, L.; van der Vegt, N.; Leon, S. *Macromolecules* **2005**, *38*, 8078−8092.
(19) Potschke, P.; Kasaliwal, G. R.; Pegel, S.; Goldel, A.; Heinrich, G. *Polymer* **2010**, *51*, 2708−2720.
(20) Potschke, P.; Pegel, S.; Petzold, G.; Alig, I.; Dudkin, S. M.; Lellinger, D. *Polymer* **2008**, *49*, 974−984.
(21) Micusik, M.; Omastova, M.; Krupa, I.; Prokes, J.; Pissis, P.; Logakis, E.; Pandis, C.; Potschke, P.; Pionteck, P. *J. Appl. Polym. Sci.* **2009**, *113*, 2536−2551.
(22) Du, F. M.; Scogna, R. C.; Zhou, W.; Brand, S.; Fischer, J. E.; Winey, K. I. *Macromolecules* **2004**, *37*, 9048−9055.
(23) Masuda, J.; Torkelson, J. M. *Macromolecules* **2008**, *41*, 5974−5977.
(24) Baets, J.; Godara, A.; Devaux, J.; Verpoest, I. *Composites, Part A* **2008**, *39*, 1756−1761.
(25) Potschke, P.; Kasaliwal, G. R.; Goldel, A. *J. Appl. Polym. Sci.* **2009**, *112*, 3494−3509.
(26) Van Der Spoel, D.; Lindahl, E.; Hess, B.; Groenhof, G. *J. Comput. Chem.* **2005**, *26*, 1701−1718.
(27) Hess, B.; Kutzner, C.; van der Spoel, D.; Lindahl, E. *J. Chem. Theory Comput.* **2008**, *4*, 435−447.
(28) Ryckaert, J. P.; Bellemans, A. *Chem. Phys. Lett.* **1975**, *30*, 123.
(29) Ryckaert, J. P.; Bellemans, A. *Discuss. Faraday Soc.* **1978**, *66*, 95.
(30) Frisch, M. J. et al. *Gaussian 09*, Revision A.1.; Gaussian Inc.: Wallingford, CT, 2009.
(31) Jorgensen, W. L.; Tirado-Rives, J. *J. Am. Chem. Soc.* **1988**, *110*, 1657−1666.
(32) Jorgensen, W. L.; Maxwell, D. S.; Tirado-Rives, J. *J. Am. Chem. Soc.* **1996**, *118*, 11225−11236.
(33) Berendsen, H. J. C.; Postma, J. P. M; Vangunsteren, W. F.; Dinola, A.; Haak, J. R. *J. Chem. Phys.* **1984**, *81*, 3684−3690.
(34) Hess, B.; Bekker, H.; Berendsen, H. J. C.; Fraaije, J. G. E. M. *J. Comput. Chem.* **1997**, *18*, 1463−1472.
(35) http://www.par-group.co.uk.
(36) Brydson, J. A. *Plastic Materials*; Butterworth: London, 1982.
(37) Henrichs, P. M.; Luss, R. H.; Scaringe, R. P. *Macromolecules* **1989**, *22*, 2731−2742.
(38) Sommer, K.; et al. *Adv. Mater.* **1991**, *3*, 590−599.
(39) Wei, C.; Srivastava, D.; Cho, K. *Nano Lett.* **2002**, *2*, 647−650.
(40) Patey, G. N.; Valleau, J. P. *Chem. Phys. Lett.* **1973**, *21*, 297.
(41) Torrie, G. M.; Valleau, J. P. *Chem. Phys. Lett.* **1974**, *28*, 578.
(42) Torrie, G. M.; Valleau, J. P. *J. Comput. Phys.* **1977**, *23*, 187.
(43) Karplus, M.; Bartels, C. *J. Phys. Chem. B* **1998**, *102*, 865−880.
(44) Bevan, D. R.; Lemkul, J. A. *J. Phys. Chem. B* **2010**, *114*, 1652−1660.
(45) Halperin, A.; Ermilov, V.; Lazutin, A. *Macromolecules* **2010**, *43*, 3511−3520.
(46) Gunsteren, W. F.; Beutler, T. C.; Bremi, T.; Ernst, R. R. *J. Phys. Chem.* **1996**, *100*, 2637−2645.
(47) Novak, B. R.; Moldovan, D.; Waldrop, G. L.; de Queiroz, M. S. *J. Phys. Chem. B* **2009**, *113*, 10097−10103.
(48) Maragakis, P.; van der Vaart, A.; Karplus, M. *J. Phys. Chem. B* **2009**, *113*, 4664−4673.
(49) Wolf, M. G.; Jongejan, J. A.; Laman, J. D.; de Leeuw, S. W. *J. Phys. Chem. B* **2008**, *112*, 13493−13498.
(50) Procacci, P.; Marsili, S.; Barducci, A.; Chelli, R.; Schettino, V. *J. Phys. Chem. B* **2006**, *110*, 14011−14013.
(51) Topf, M.; Richards, W. G. *J. Am. Chem. Soc.* **2004**, *126*, 14631−14641.
(52) Brady, J. W.; Schmidt, R. K.; Teo, B. *J. Phys. Chem.* **1995**, *99*, 11339−11343.
(53) Rosenberg, J. M.; Kumar, S.; Bouzida, D.; Swendsen, R. H.; Kollman, P. A. *J. Comput. Chem.* **1992**, *13*, 1011−1021.